Parameter Study of a Continuously Stratified Model of the Ideal-Fluid Thermocline*

RUI XIN HUANG

Department of Physical Oceanography, Woods Hole Oceanographic Institution, Woods Hole, Massachusetts

(Manuscript received 9 November 1998, in final form 11 August 1999)

ABSTRACT

The parameter sensitivity of a continuously stratified model of the ideal-fluid thermocline in the subtropical gyre interior is studied. A one-dimensional advection–diffusion model is used to set up a background stratification that can provide both the potential vorticity function for the unventilated thermocline and the mixed layer depth used in the ideal-fluid thermocline model. The wind-driven circulation is treated as a perturbation to this background stratification. Although the perturbation solution excludes mixing/diffusion, the dynamic effect of diapycnal mixing is included in the unperturbed solution; therefore, the ideal-fluid solution should correspond to a nonzero diffusion solution for the wind-driven and thermohaline circulation in the ocean.

It is shown that the model can reproduce the thermocline structure, which corresponds to either finite or infinitely weak mixing. Under the extreme weak diffusion limit, the model produces a thermocline that looks like a step function in the stratification, which separates the wind-driven gyre above it and the stagnant abyssal water underneath it.

It is shown that the subduction rate and production of mode water with low-potential vorticity are closely related to the stratification (or the potential vorticity) of the unventilated thermocline, the geometry of the mixed layer, the Ekman pumping rate, and the orientation of the intergyre boundary. Changes in the structure of the thermocline in response to different upper boundary conditions are explored. It is found that cooling and southward migration of the jet stream induce the production of low potential vorticity mode water, while changes in the vertical density profile have an appearance like the second baroclinic mode.

1. Introduction

The wind-driven circulation is a dominant component of the currents in the upper ocean. A traditional way of studying the circulation in the upper ocean is to separate the wind-driven circulation from currents driven by other mechanisms, such as tides and thermohaline circulation. Over the past half century theories of the wind-driven circulation have evolved to quite a comprehensive level.

The simplest model is the reduced-gravity model, widely used for the past 50 years. Much effort has been devoted to developing theory of the wind-driven circulation, or, as it is sometimes called, the thermocline theory. However, it has taken many decades of research effort to develop wind-driven circulation models with more than one moving layer. Two approaches have been developed from the beginning. Robinson and Stommel (1959) proposed a thermocline theory in which diapycnal mixing was explicitly included. At the same time, Welander (1959) proposed a theory in which the fluid in the wind-driven gyre is treated as an ideal fluid, that is, without mixing and diffusion.

During the two decades after the publication of these pioneering papers many people worked on the thermocline theories. The first approach proposed by Robinson and Stommel (1959) was much more attractive because it seemed to have the promise of a complete solution in which the wind-driven and thermohaline circulation with diapycnal mixing were included explicitly. Due to the strong nonlinear nature of the problem, no simple analytical solutions exist. To overcome this difficulty, the similarity approach has been widely used. The similarity solutions belong to the more general approach of finding a solution to differential equations based on the invariant group (e.g., Filippov 1968; Oliver 1986). For a given set of differential equations, there is a systematic way to find the invariant group. As long as this invariant group is found, all similarity solutions can be represented as members of this family.

A major disadvantage of this group theory approach is that solutions found in this way generally do not satisfy boundary conditions imposed on the model from physical considerations. Without satisfying these important dynamic boundary conditions, such as the Ek-

* Woods Hole Oceanographic Institution Contribution Number 9868.

Corresponding author address: Rui Xin Huang, Department of Physical Oceanography, Woods Hole Oceanographic Institution, Woods Hole, MA 02543
E-mail: rhuang@whoi.edu

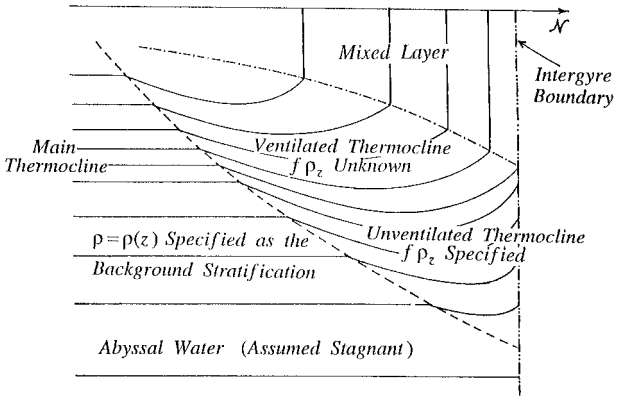

FIG. 1. Schematic structure of the ideal-fluid thermocline model in a subtropical basin. The dashed line indicates the base of the wind-driven gyre, and the dot–dashed line indicates the interface between the mixed layer and the thermocline.

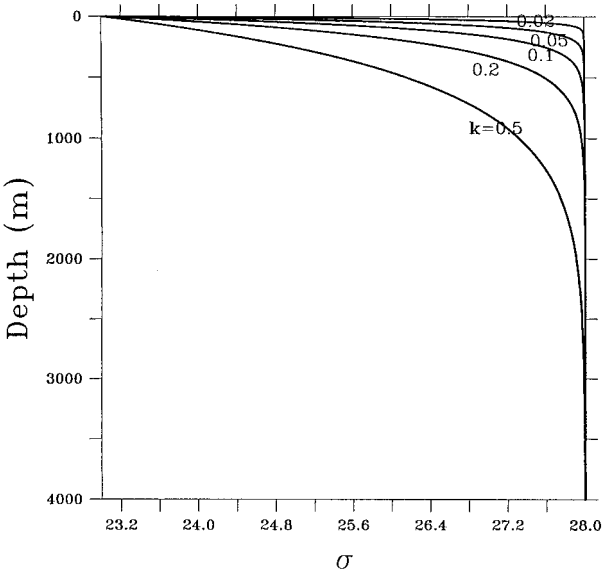

FIG. 2. Background stratification generated by a one-dimensional advection–diffusion model; $w = 10^{-5}$ cm s^{-1}.

man pumping condition, the physical meaning of such solutions is not very clear. Thus, regardless of the great effort spent on finding similarity solutions, little progress has been made.

On the other hand, the ideal-fluid thermocline approach proposed by Welander (1959) seemed not very attractive in the beginning, and most people (except Welander himself) did not want to do something less complete than a model with everything, especially with vertical mixing. However, it turned out that this seemingly incompetent approach of treating the wind-driven circulation as an ideal-fluid perturbation to a given stratification is rather fruitful, just as successful as all other wind-driven circulation models.

Starting from the beginning of the 1980s, there was a major breakthrough in the development of wind-driven circulation theories. Most importantly, fully nonlinear solutions without any a priori similarity constraints have been discovered, including the potential homogenization theory by Rhines and Young (1982) and the ventilated thermocline theory by Luyten et al. (1983a). These solutions have provided us with deep insight to the physics of the wind-driven circulation, such as the discovery of different dynamic zones in the upper oceans, that is, the ventilated thermocline, the unventilated thermocline, the shadow zone, the pool zone, and the subduction zone.

Theories of potential vorticity homogenization and the ventilated thermocline have been combined and extended into a model for the continuously stratified ocean by Huang (1988, 1990), including a mixed layer on top and a continuously stratified unventilated water column below the ventilated thermocline. The model is forced by background stratification and surface forcing diagnosed from a climatelogical dataset; thus, the model is capable of reproducing the wind-driven circulation in the oceans in a quite realistic way, as discussed by Huang (1990), Huang and Russell (1994), and Huang and Qiu (1998). The recent study based on tracer release experiments has further confirmed that mixing in the upper ocean is very weak, on the order of 0.1 cm^2 s^{-1} in the open oceans (Ledwell et al. 1993). Therefore, the ideal-fluid thermocline model that ignores mixing in the perturbation part of the solution does seem to be a good approach.

Although these studies have helped us to understand the wind-driven circulation in present-day oceans, it is not clear how the circulation would change in response to changes in the forcing conditions and other parameters. Luyten et al. (1983b) carried out a parameter study for the ventilated thermocline model; however, their study was based on the original version of the ventilated thermocline, so the dynamic role of the mixed layer and the unventilated thermocline was excluded. In some sense, application of the original ventilated thermocline model to the three major basins, the North Atlantic by Luyten et al. (1983a), the North Pacific by Talley (1985), and the South Pacific by de Soeke (1987), provides a useful glimpse to the model's behavior in an immense parameter space. In addition, recent studies by Liu et al. (1993) and Lionello and Pedlosky (1999) also highlighted some aspects of the model's behavior. Up to now, however, the behavior of a continuously stratified model under different climate conditions remains unclear. Thus, the goal of this study is to examine the parameter sensitivity of the model to the basic parameters and forcing conditions.

The model used here is a continuously stratified model of the ideal-fluid thermocline, which is forced by idealized surface forcing. The model formulation is briefly discussed in section 2. In section 3, the model's sensitivity to changes in basic parameters and geometry is studied.

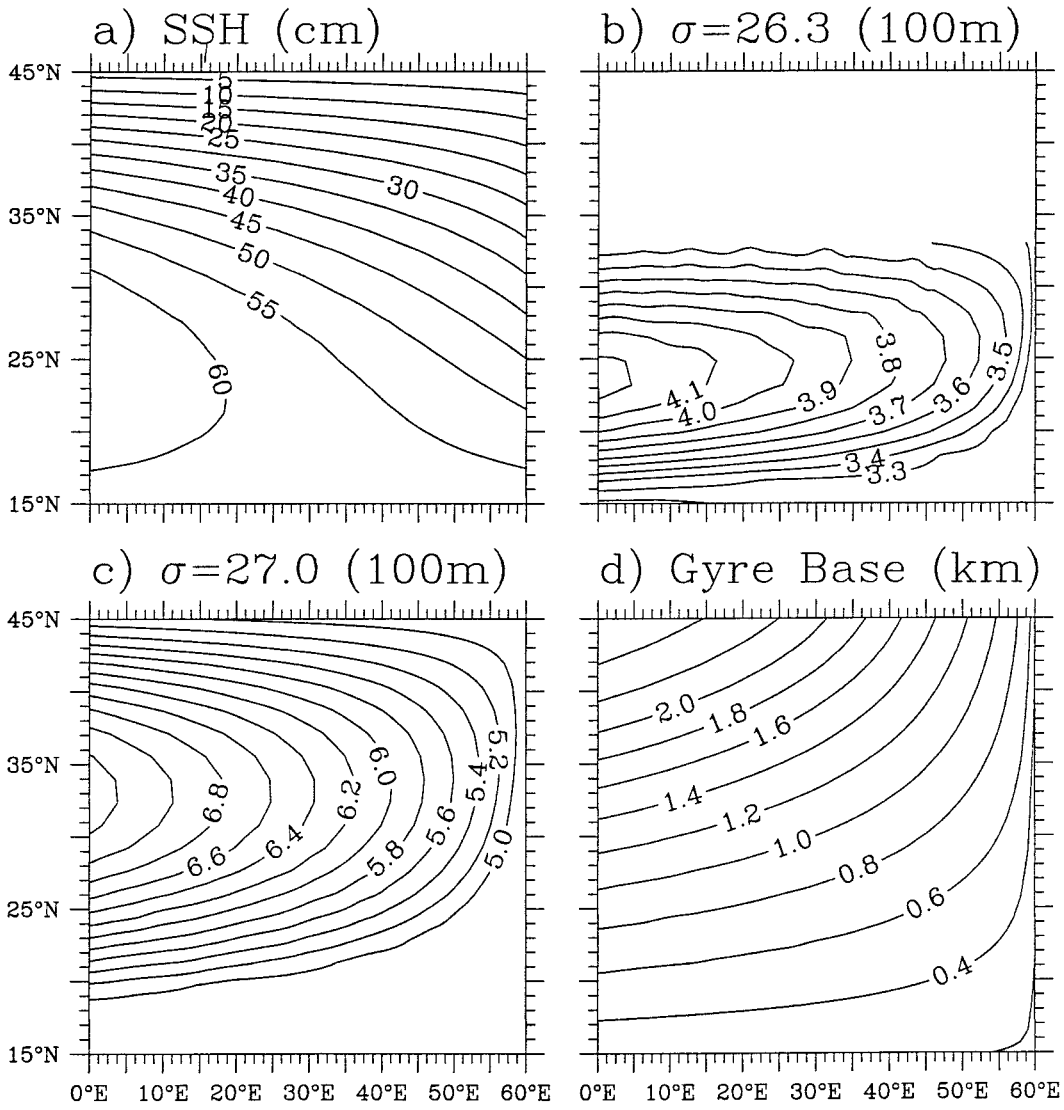

FIG. 3. Mean circulation fields for the case with $\kappa = 0.3$ cm^2 s^{-1} (a) Sea surface elevation in centimeters; (b) depth of isopycnal surface $\sigma = 26.3$, in 100 m; (c) depth of isopycnal surface $\sigma = 27.0$, in 100 m; and (d) depth of the base of the wind-driven gyre, in kilometers.

2. Model formulation

The formulation used in this study is adapted from earlier study by Huang (1988) and Huang and Russell (1994). The three-dimensional structure of the wind-driven gyre can be described in terms of a scalar function, the Bernoulli function

$$B = P + \rho gz. \tag{1}$$

For large-scale circulation geostrophy is a good approximation, so the horizontal momentum equations are reduced to

$$f\overline{\rho}v = B_x, \qquad f\overline{\rho}u = -B_y, \tag{2}$$

and the vertical momentum equation degenerates to the hydrostatic relation

$$B_\rho = gz, \tag{3}$$

where the subscript ρ indicates a partial derivative with respect to ρ. The linear vorticity equation is

$$\beta v z_\rho = f w_\rho. \tag{4}$$

Using (2), (3), (4) to eliminate v and z leads to

$$B_{\rho\rho}B_x = \frac{g\overline{\rho}f^2}{\beta}w_\rho. \tag{5}$$

Integrating this equation over $[\rho^s, \rho^b]$, where $\rho^s(x, y)$ is the given mixed layer density distribution and $\rho^b(x, y)$ is the unknown free boundary separating the moving water from the stagnant abyssal water, gives

$$-\int_{\rho^s}^{\rho^b} B_\rho^2\, d\rho + \int_{\rho^{se}}^{\rho^{be}} B_\rho^{e2}\, d\rho + \int_{\rho^{be}}^{\rho^b} B_\rho^{a2}\, d\rho = \frac{2g\overline{\rho}f^2}{\beta}\int_x^{x^e} w_e\, dx. \quad (6)$$

We also assume that along the eastern boundary the base of moving water is at the base of the mixed layer, thus $\rho^{be} = \rho^{se}$ and the second integral on the left-hand side of (6) vanishes. From these equations, the calculation of the wind-driven gyre in the subtropical basin is reduced to solving the following free-boundary value problem in density coordinates

$$B_{\rho\rho} = \frac{fg}{Q(B, \rho)}, \quad (7)$$

where $Q(B, \rho)$ is the potential vorticity function. For the unventilated thermocline, $Q = f_0\rho_z$, where f_0 is the Colioris parameter at the northern boundary of the subtropical gyre and ρ_z is the given background stratification. For water in the pool region, that is, water coming from the western boundary, Q is set to the value at the eastern edge of the pool (Rhines and Young 1982; Dewar 1986). For water below the base of the wind-driven gyre, $Q^a = f\rho_z$, hereafter the superscript a depicts the abyssal water. This equation is subject to constraints

$$B_\rho = -gh(x, y) \quad \text{at } \rho = \rho^s; \quad (8)$$

$$B = B^a(\rho), \qquad B_\rho = B_\rho^a(\rho) \quad \text{at } \rho = \rho^b, \quad (\rho^b \text{ is unknown}), \quad (9)$$

$$-\int_{\rho^s}^{\rho^b} B_\rho^2\, d\rho + \int_{\rho^{se}}^{\rho^b} B_\rho^{a2}\, d\rho = \frac{2g\overline{\rho}f^2}{\beta}\int_x^{x^e} w_e\, dx. \quad (10)$$

Note that the second integral starts from ρ^{se}, not ρ^s, because surface density at the eastern boundary along a zonal section may be different from the surface density at an interior grid point. Constraint (10) is the generalized Sverdrup relation for a continuously stratified ocean.

The subtropical basin interior, excluding the western boundary region, is divided into $M \times N$ stations, where M is the number of the isopycnal outcrop lines and N is the number of stations along each outcrop line. The solution is calculated by solving the above free boundary value problem station by station.

The model ocean is a rectangular basin of $60° \times 30°$ (from 15° to 45°N), mimicking the subtropical North Atlantic. Input data required for the calculation include an Ekman pumping rate, a mixed layer density and depth distribution, and the background stratification. In this study we will use an Ekman pumping forcing that has a simple sinusoidal distribution in the meridional direction,

$$w_e = -1.0 \times 10^{-4} \sin\left(\pi\frac{y - y_s}{\Delta y}\right) \quad \text{cm s}^{-1}, \quad (11)$$

where $y_s = 15°$N is the southern boundary of the model basin, $\Delta y = 30°$ is the meridional range of the model basin.

Although the wind-driven circulation and the thermohaline circulation in the oceans are coupled together nonlinearly, a traditional approach in oceanography has been to treat these two components separately. Separating one component of a nonlinear system from other components has its advantages and disadvantages. This is certainly true for the traditional approach of separating the wind-driven circulation from the thermohaline circulation. In this study we will demonstrate that separating the wind-driven circulation from the thermohaline circulation does help us to simplify the problem and obtain very useful information about the physical structure of the circulation in the upper ocean.

The fundamental assumption made in all simple theoretical models of the wind-driven circulation is that a background stratification, which is controlled by external dynamics, is specified a priori. For example, in a reduced-gravity model the density jump cross the interface and the upper-layer thickness along the eastern boundary must be specified as external parameters of the model. In the ventilated thermocline theory by Luyten et al. (1983a), the density jumps across each interface and the layer thicknesses along the eastern boundary must be specified a priori. Obviously, changes in these parameters can affect the wind-driven circulation in these models. Although such models require some kind of information about the stratification to be specified a priori, they do provide clear dynamic pictures of the circulation in the upper ocean; thus they have been used successfully in many cases.

For the study of the three-dimensional structure of the wind-driven circulation in the upper ocean, we need to specify the background stratification, as discussed by Huang (1988, 1990). It is assumed that potential vorticity in the unventilated thermocline is homogenized toward its value along the intergyre boundary (Rhines and Young 1982). In addition, the calculation of the ventilated layers requires the specification of stratification along the eastern boundary for the ventilated layers. Note that we assume that along the eastern boundary the base of wind-driven gyre is at the base of the mixed layer, so all of the isopycnal surface below the mixed layer is inside the shadow zone, where stratification is set by the input background stratification [see Huang (1990) for the details]. On the other hand, potential vorticity in the ventilated thermocline cannot be specified a priori. Instead, it is calculated as a part of the solution (Fig. 1).

In this model density is assumed vertically uniform in the mixed layer. Since there is no seasonal cycle in the model, winter mixed layer density and depth are used, instead of annual mean values. On the other hand, the annual mean Ekman pumping rate is used to force the model. These assumptions are based on the Stommel demon (Stommel 1979); that is, the subduction process

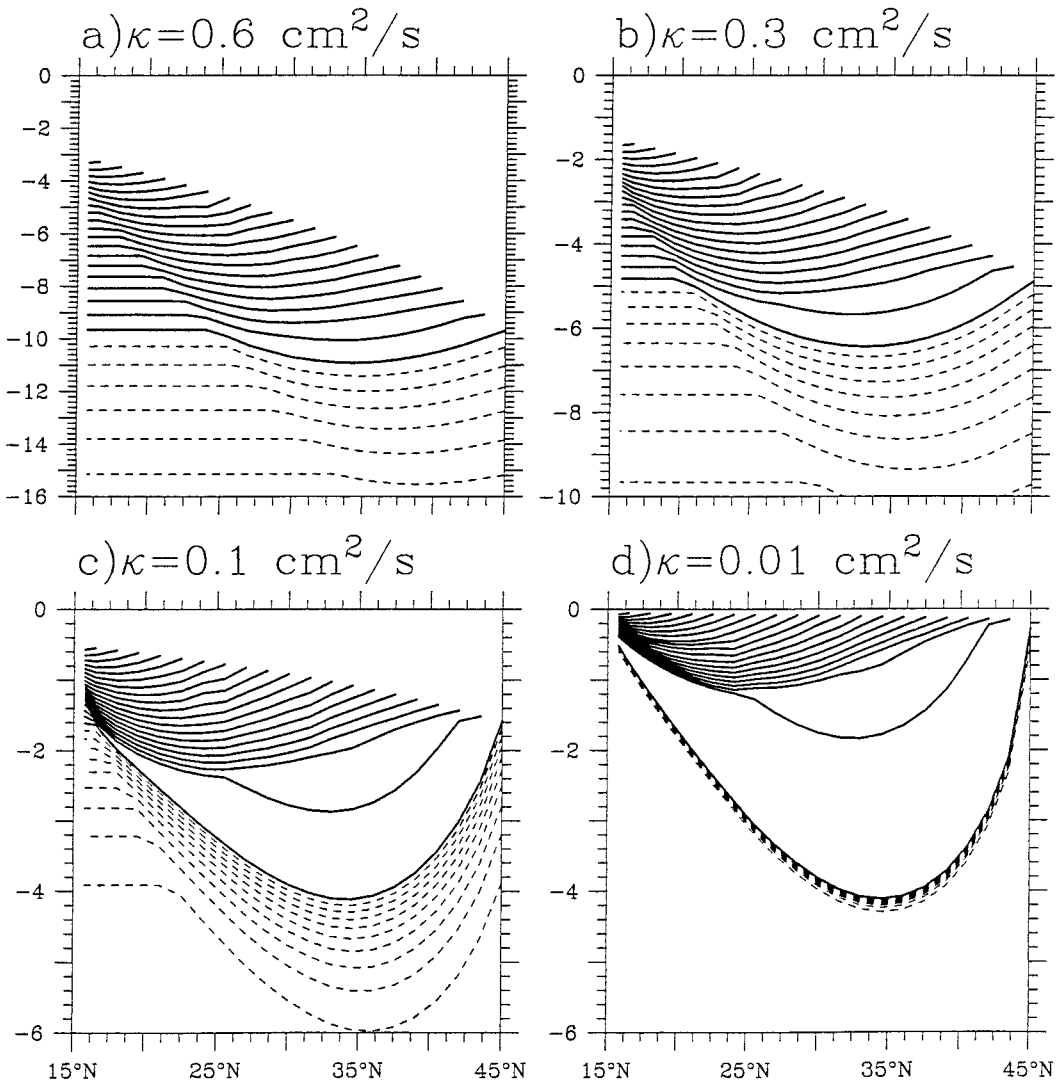

FIG. 4. Isopycnal sections taken along the outer edge of the western boundary (5°E), with the solid lines depicting the ventilated thermocline and the dashed lines depicting the unventilated thermocline, with an interval of $\Delta\sigma = 0.1$. The blank portion in the upper ocean indicates the mixed layer where density is vertically uniform.

automatically selects mixed layer properties of late winter. As shown in Fig. 1, the base of the wind-driven gyre varies over a wide range of depth and density. The depth of this interface is unknown and it is part of the solution we are seeking from the model. Below this interface stratification is specified as input. Although potential vorticity in the unventilated thermocline is specified, the exact depth of each unventilated layer is unknown. Most importantly, the potential vorticity in the ventilated thermocline is unknown, and this is the most critical part of the solution from the model.

In short, the wind-driven circulation theories treat the circulation in the upper ocean as perturbations to a vertical stratification profile specified by some external models. Note that the perturbation is strongly nonlinear and of finite amplitude. In particular, the stratification, or the potential vorticity, in the ventilated thermocline is entirely generated from the wind-driven circulation dynamics, and it can be dramatically different from the background stratification specified.

Although no mixing or diffusion is explicitly included in the perturbation part of the solution, mixing and diffusion have been included in the background stratification implicitly. Therefore, the so-called ideal-fluid thermocline model is not equivalent to setting the mixing to be infinitely small in a model that includes mixing explicitly. In fact, the ideal-fluid thermocline model actually corresponds to the circulation in the oceans with finite amount of mixing.

The background stratification used in this study is calculated by assuming a simple one-dimensional advection–diffusion balance

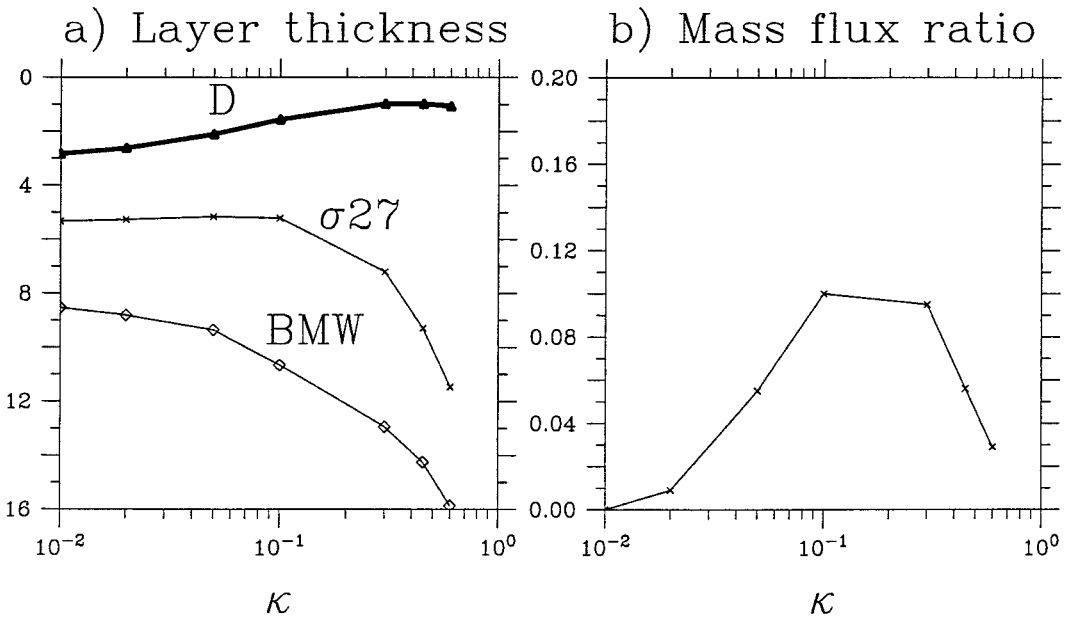

FIG. 5. (a) Layer depth at the edge of the western boundary as a function of the mixing rate κ: D is the thickness of the first ventilated layer, taken at 43.5°N, $\sigma 27$ indicates the depth of the $\sigma = 27.0$ isopycnal surface, and BMW indicates the base of moving water; both these depths are taken at 30°N. (b) Unventilated mass flux ratio calculated along the 30°N section.

$$w\rho_z = \kappa\rho_{zz}, \tag{12}$$

where $w = 1.0 \times 10^{-5}$ cm s^{-1} is a constant upwelling velocity and $\kappa = 0.01$–0.6 cm^2 s^{-1} is the vertical diffusivity. This equation yields an exponential density profile. Using density boundary conditions of $\rho = 23.0$ at $z = 0$ and $\rho = 28.0$ at the seafloor $z = -5$ km, the density profile can be calculated accordingly. This density profile provides the potential vorticity function for the unventilated thermocline. In addition, this profile will also be used as the resting level along the eastern boundary for the ventilated layers.

The one-dimensional advection–diffusion balance used to generate the stratification in this study is just a convenient way to get such a stratification. Any reasonable stratification can be used. In particular, uniform stratification can be used instead. The reason to choice the advection–diffusion model is because the model generates stratification that has an exponential profile mimicking the stratification in the oceans.

As κ is reduced, a strong density front is formed near the upper surface (Fig. 2). Apparently, the stratification in the oceans corresponds to the density profile with $\kappa \approx 0.1$–0.3 cm^2 s^{-1}. The cases of $\kappa \leq 0.1$ cm^2 s^{-1} represent the theoretical limit of extremely weak diapycnal mixing. For example, when $\kappa = 0.01$ cm^2 s^{-1}, the corresponding scale height $h = \kappa/w = 10$ m. This corresponds to a very thin thermal boundary layer near the upper surface of the model ocean. Such cases with a weak mixing rate may be far from the realistic parameter regime of oceans; however, these cases are of theoretical interest on their own.

We will also assume that the mixed layer density is a linear function of latitude

$$\sigma = 25 + 2\frac{y - y_s}{y_n - y_s}, \tag{13}$$

where $y_s = 15$°N and $y_n = 45$°N are the southern and northern boundaries of the model basin. The mixed layer depth is set to the resting level of the corresponding isopycnal in the eastern boundary. The model has 20 ventilated layers, with an isopycnal interval of $\Delta\sigma = 0.1$, i.e., $\sigma = 27.0, 26.9, 26.8, \cdots, 25.2, 25.1, 25.05$. (Note that the difference between the last two isopycnals is 0.05, so that the last outcrop line is within the subtropical gyre.)

3. Parameter sensitivity of the model

Under these boundary conditions, the wind-driven circulation in the subtropical basin can be calculated according to the algorithm described by Huang (1988) and Huang and Russell (1994). The solution corresponding to $\kappa = 0.3$ cm^2 s^{-1} is presented in Fig. 3. The anticyclonic gyre is depicted by the depth maps of isopycnal surface $\sigma = 26.3$, which outcrops at 33°N, and $\sigma = 27.0$, which outcrops along the intergyre boundary. The depth of the $\sigma = 27.0$ interface reaches to more than 700 m in the middle of the western boundary, which is close to the depth of the main thermocline observed in the oceans. The map of the sea surface elevation indicates an eastward flow in the mixed layer for the most of the gyre, with a few contours being

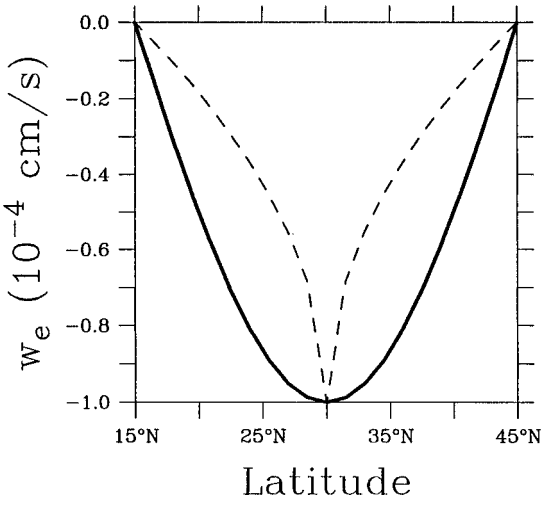

FIG. 6. Meridional distribution of the Ekman pumping rate: the solid line depicts the profile used in standard cases, the dashed line represents a special case.

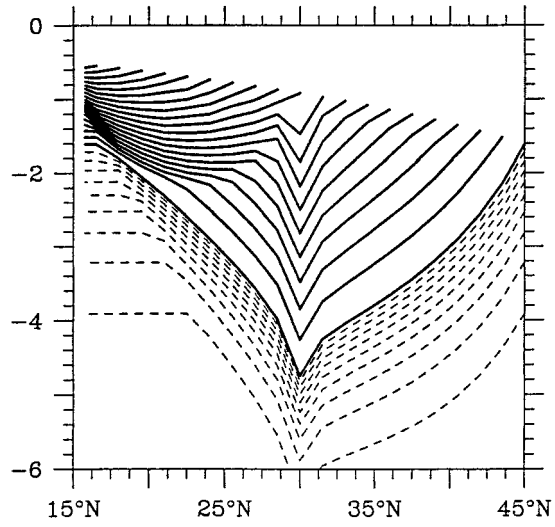

FIG. 7. An isopycnal section taken from the case with a special form of Ekman pumping velocity, depicted by the dashed line in Fig. 6, along the outer edge of the western boundary (5°E), with the solid lines depicting the ventilated thermocline and the dashed lines depicting the unventilated thermocline; contour interval $\Delta\sigma = 0.1$. The blank area in the upper ocean indicates the mixed layer.

closed through the western boundary in the southwestern corner. The flux into the eastern boundary is due to the specific boundary condition used in this model, and the reader is referred to Huang (1990) for the detail of the eastern boundary condition. The base of the wind-driven gyre extends to about 2.4 km, which is very close to the base of the subtropical gyre in the North Atlantic (Huang 1990).

a. Sensitivity to the mixing rate

For cases of strong mixing, the main thermocline is very thick; however, as κ is reduced, the thermocline becomes progressively sharper. The main thermocline for the case with $\kappa = 0.6$ cm^2 s^{-1} seems to be very diffusive (Fig. 4a). On the other hand, the main thermocline produced with $\kappa = 0.1$–0.3 cm^2 s^{-1}, as plotted in Figs. 4b,c, is relatively sharp and resembles the main thermocline observed in the oceans. As κ is reduced to 0.01 cm^2 s^{-1}, the main thermocline becomes a step-function like a thin internal surface of density discontinuity (Fig. 4d). A remarkable feature in these solution is the low-potential vorticity mode water formed in the first ventilated layer. As the vertical diffusivity is gradually reduced, this low potential vorticity layer becomes more outstanding. This is consistent with the recent analysis by Lionello and Pedlosky (1999), who studied a ventilated thermocline model with up to 100 moving layers and demonstrated that low potential mode water always appears in the first ventilated layer. The relation between the potential vorticity of the mode water and parameters of the model will be examined in detail shortly.

These examples show that the ideal-fluid thermocline model can be used to describe wind-driven circulation in the upper ocean over a wide range of the diffusive parameter, from the strongly diffusive limit to the extremely weakly diffusive limit. The sharp density front appearing in our model with low mixing rate is very similar to the density discontinuity found in other idealized models with very low mixing rates (e.g., Salmon 1990; Samelson and Vallis 1995).

There has been some confusion in the literature about the applicability of the ideal-fluid thermocline to the oceans. For example, Salmon (1990) claimed that "it is

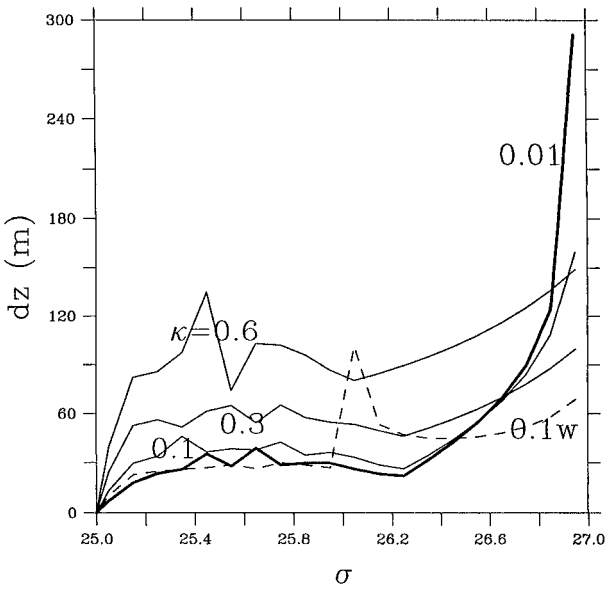

FIG. 8. Maximum potential thickness for each isopycnal surface, where κ is the vertical diffusivity and 0.1 *w* indicates the result generated by the special Ekamn pumping profile in Fig. 7.

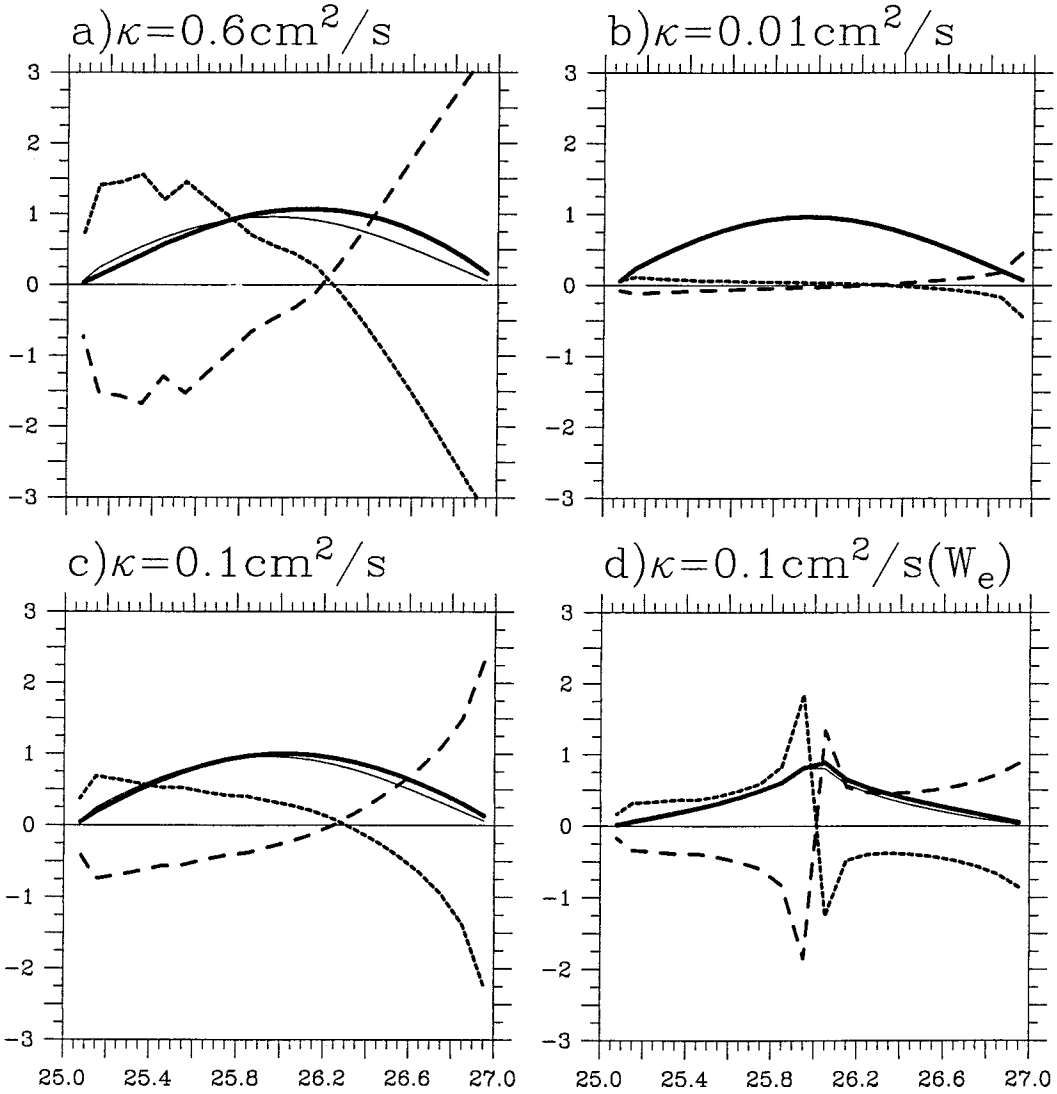

FIG. 9. Subduction rate balance at each isopycnal outcrop band ($\Delta\sigma$ = 0.1, in Sverdrups, 10^6 m^3 s^{-1}). The solid lines are the subduction rate, long-dashed lines are the contribution due to the western boundary outflow, the dotted lines are the contribution due to the meridional mass flux convergence, and the thin solid lines are the contribution due to Ekman pumping: (a) κ = 0.6 cm^2 s^{-1}, (b) κ = 0.01 cm^2 s^{-1}, (c) κ = 0.1 cm^2 s^{-1}, and (d) κ = 0.1 cm^2 s^{-1}, with the special-profile Ekman pumping.

impossible to explain the thermocline structure within the subtropical gyre on the basis of ideal thermocline theory (i.e., without invoking temperature diffusion).'' Our examples clearly show that his statement is inaccurate. The essential point is that the so-called ideal-fluid thermocline theory treats the wind-driven circulation as a perturbation to the background stratification (or the potential vorticity) set up by an external mechanism. There is, indeed, no mixing or diffusion in the perturbation solution itself. However, the dynamic role of mixing is implicitly included through the specification of the background stratification, that is, the potential vorticity function for the unventilated thermocline. Thus, the dynamic role of both horizontal and vertical mixing in the ocean is included in the solution. As a result, the ideal-fluid thermocline theory can be applied to the real oceans where the mixing rate is small, but finite. In fact, the ideal-fluid thermocline theory has been applied to three basins: the North Atlantic (Huang 1990), the North Pacific (Huang and Russell 1994), and the South Pacific (Huang and Qiu 1998). In these studies the background stratification is diagnosed from the Levitus climatology, and the structure calculated from the model compares favorably with other diagnostic studies based on observations.

On the other hand, much effort was devoted to solving the thermocline model including vertical mixing; however, such a model may not be a good choice for the following reasons: First, no nonsimilarity solution has been found for such a model. Since similarity solutions do not satisfy some important boundary conditions, their

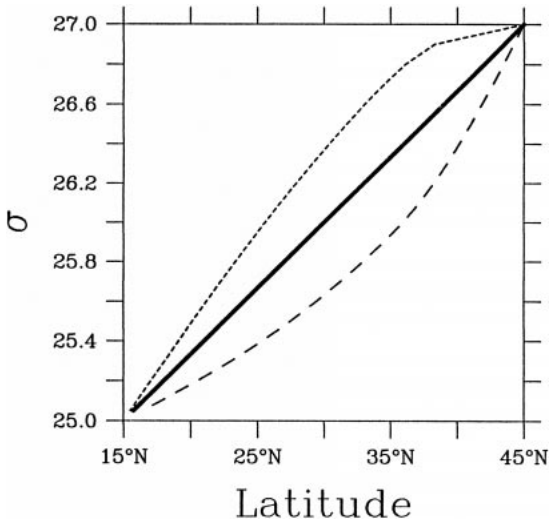

FIG. 10. Meridional distribution of the mixed layer density: the solid line for the standard linear profile, the dotted line for the case with cooling, and the long-dashed line for the case with warming.

physical meaning is not clear. Second, a model involving vertical mixing only is incomplete because horizontal mixing may play a very important role in setting up the potential vorticity balance in a closed basin. Thus, a solution from a model without horizontal mixing may be quite different from the circulation in the oceans. Note that the solution based on potential vorticity homogenization has included along-isopycnal mixing implicitly through the specification of the potential vorticity.

As the mixing rate is gradually reduced, the thermocline approaches a nondiffusive limit. As shown in Fig. 5a, the base of the wind-driven gyre reaches a limit of 860 m, and the base of the ventilated thermocline ($\sigma = 27.0$) also approaches a limit depth of about 540 m. At the same time the thickness of the upper ventilated layer also gradually increases and approaches its limit.

Another interesting phenomenon is that the mass flux in the unventilated thermocline is greatly reduced when the mixing rate is reduced. In order to demonstrate this, we introduce the unventilated mass ratio, defined as the mass flux in the unventilated thermocline divided by the barotropic mass flux at a given latitude. In this study, we choose 30°N, the middle latitude of the gyre, for the calculation. Although for $\kappa \geq 0.1$ cm^2 s^{-1} the unventilated mass ratio fluctuates around a level of 10%, it gradually diminishes as κ is reduced. For $\kappa = 0.01$ cm^2 s^{-1}, this mass flux ratio is practically zero. Thus, the horizontal mass transport of the wind-driven circulation is all confined above the base of the ventilated thermocline, $\sigma = 27.0$. Below this isopycnal surface there is virtually no motion.

The most important phenomenon is the low potential vorticity water formed near the intergyre boundary. As κ is gradually reduced, the contrast between the potential vorticity on isopycnals close to 27.0 and on isopycnal surfaces with density much smaller than 27.0 becomes remarkably greater. For the case with $\kappa = 0.6$ cm^2 s^{-1}, the difference in potential vorticity is relatively small. However, for the case with $\kappa = 0.01$ cm^2 s^{-1}, low potential vorticity is confined to the lowest two ventilated layers (Fig. 4d).

b. The relation between the base of the ventilated thermocline and base of the wind-driving gyre

A basic assumption within our model is that in each unventilated layer potential vorticity is homogenized toward its value along the intergyre boundary, so potential vorticity function is $q = f_0\rho_z^a = f_0/z_\rho^a$, where f_0 is the Coriolis parameter along the intergyre boundary, ρ_z^a is the background stratification. Integrating (7) gives the isopycnal depth at an interior point

$$B_\rho = B_\rho^0 + \frac{fg}{f_0} Z(\rho, \rho_0), \qquad Z(\rho, \rho_0) = \int_{\rho_0}^{\rho} z_\rho^a \, d\rho, \tag{14}$$

where $B_\rho^0 = gz^0$ and z^0 is the depth of the isopycnal ρ_0, which separates the ventilated thermocline and the unventilated thermocline. Similarly, along the eastern boundary we have

$$B_\rho^e = B_\rho^{e0} + gZ(\rho, \rho_0), \tag{15}$$

where $B_\rho^{e0} = -gh_0$, and $-h_0$ is the depth of isopycnal ρ_0 at the eastern boundary.

According to (9), B_ρ should match B_ρ^e at $\rho = \rho^b$ so that

$$B_\rho^0 = Z(\rho, \rho^0)g(1 - f/f_0) + B_\rho^0. \tag{16}$$

Finally, we have the simple relation

$$B_\rho^b = B_\rho^0 \frac{f_0}{f_0 - f} + \frac{f - 2f_0}{f - f_0} B_\rho^{e0}. \tag{17}$$

Thus, the base of the wind-driven gyre is proportional to the depth of the base of the ventilated thermocline, with a factor that depends on the latitude only. Since potential vorticity is constant within each unventilated layer, when the model solution changes in response to variability in forcing and parameter, the unventilated layer should move up and down with the same displacement. Furthermore, the base of the wind-driven gyre moves in the same direction as the deep ventilated isopycnals; that is, downward movement of deep ventilated isopycnal corresponds to deepening of the wind-driven gyre.

c. Formation of low-potential-vorticity mode water

Low potential vorticity associated with subtropical mode water is observed in the world oceans, especially the North Atlantic and the North Pacific (e.g., McCartney 1982). The formation of such low potential vorticity has been linked to strong winter cooling that creates a thick layer of mode water with nearly homogenized properties. However, it is not clear how much other

gyre-scale dynamics affect the potential vorticity of the mode water. In this study we will examine several dynamic factors that control the potential vorticity of mode water.

For simplicity, we assume that the background stratification is constant for all unventilated layers. Along the eastern boundary, integration of (7) leads to

$$B_\rho^e = -gh_0 + \frac{g}{\rho_z^a}(\rho - \rho^0). \tag{18}$$

At a station in the ocean interior, the corresponding relation is

$$B_\rho = B_\rho^0 + \frac{fg}{f_0\rho_z^a}(\rho - \rho^0), \tag{19}$$

By matching B_ρ at the base of moving water ρ^b, one finds

$$\rho^b - \rho^0 = \frac{f_0\rho_z^a}{g(f_0 - f)}(B_\rho^0 + gh_0). \tag{20}$$

Since we assume $\rho^{se} = \rho^s$, the integrals on the left-hand side of (10) are

$$\int_{\rho^s}^{\rho^b} B_\rho^2\, d\rho = \frac{f_0\rho_z^a}{3fg}\left[\left(\frac{f_0}{f_0 - f}B_\rho^0 + \frac{f}{f_0 - f}gh_0\right)^3 - B_\rho^{0^3}\right] + \int_{\rho^s}^{\rho^0} B_\rho^2\, d\rho, \tag{21}$$

$$\int_{\rho^s}^{\rho^b} B_\rho^{a^2}\, d\rho = \frac{\rho_z^a}{3g}\left[\left(\frac{f_0}{f_0 - f}B_\rho^0 + \frac{f}{f_0 - f}gh_0\right)^3 + (gh_0)^3\right] + \int_{\rho^s}^{\rho^0} B_\rho^{a^2}\, d\rho, \tag{22}$$

where the last integrals on the right-hand side of (21), (22) are high-order small terms and can be neglected in the following analysis. Thus, the generalized Sverdrup constraint is

$$\left[1 - \left(1 - \frac{f}{f_0}\right)^{-2}\right]X^3 - \frac{3ff_0}{(f_0 - f)^2}gh_0X^2 - \frac{3f^2}{(f_0 - f)^2}g^2h_0^2X = \left(-\frac{f}{f_0} + \frac{f^3}{f_0(f_0 - f)^2}\right)g^3h_0^3 + \frac{6f^3g^2\overline{\rho}}{f_0\beta\rho_z^a}\int_x^{x_e} w_e\, dx, \tag{23}$$

where $X = B_\rho^0$. This cubic equation can be solved numerically; however, we can simplify it by omitting the small terms. Since $f_0 - f \approx \beta\delta y$, $\delta y = y_0 - y$ (y_0 is the intergyre boundary), this equation is reduced to

$$X^3 = -g^3h_0^3 - \frac{6g^2\overline{\rho}\beta\delta y^2}{\rho_z^a}\int_x^{x_e} w_e\, dx. \tag{24}$$

If we assume that the mixed layer thickness, h_0, is zero, this leads to the expression for the upper ventilated layer thickness discussed by Huang (1988):

$$\Delta z = \left(\frac{6\overline{\rho}\beta}{g\rho_z^a}(y - y_0)^2\right)^{1/3}[w_e(x_e - x)]^{1/3}, \tag{25}$$

where w_e is the Ekman pumping velocity at this outcrop line. Assume a Taylor expansion of the Ekman pumping velocity

$$w_e = w_d\delta y, \tag{26}$$

where $w_d = dw_e/dy$ is the meridional gradient of the Ekman pumping rate, $\delta y = y - y_0$. In addition, we assume that the mixed layer density is a linear function of latitude

$$\rho = \rho_0 + \frac{d\rho^s}{dy}\delta y, \tag{27}$$

where $d\rho^s/dy$ is the meridional gradient of the mixed layer density. Then, potential vorticity of the first ventilated layer is

$$q = f\frac{\Delta\rho}{\Delta z} = f_0\frac{d\rho^s}{dy}\left(\frac{g\rho_z^a}{6\rho_0\beta w_d}\right)^{1/3}(x_e - x)^{-1/3}, \tag{28}$$

Note that potential vorticity is finite near the intergyre boundary, as discussed by Huang (1988). Accordingly, a weak meridional mixed layer density gradient and a strong meridional gradient of the Ekman pumping rate can lead to low potential vorticity in the mode water. On the other hand, this equation also suggests that strong stratification would lead to high potential vorticity, and it is clearly in contradiction to the results shown in Fig. 4.

This inconsistency is due to neglecting the mixed layer depth contribution in (24). For $\delta y \ll O(1)$, the Ekman pumping term is very small, and the solution to (24) can be obtained by a perturbation technique

$$X + gh_0 \approx -\frac{2\overline{\rho}\beta\delta y^2}{h_0^2\rho_z^a}w_e\Delta x, \qquad \Delta x = x_e - x. \tag{29}$$

Thus, the thickness of the upper ventilated layer is

$$\Delta z = -\frac{X + gh_0}{g} \approx \frac{2\overline{\rho}\beta\delta y^2}{gh_0^2\rho_z^a}w_e\Delta x. \tag{30}$$

If we assume that the background stratification is constant, including the mixed layer, the mixed layer depth is related to its density

$$g^2h_0^2 = \left(\frac{g\Delta_m\rho}{\rho_z^a}\right)^2, \tag{31}$$

where $\Delta_m\rho$ is the density difference between the given isopycnal and the minimum density on the surface along the southern edge of the basin. In addition, we neglect a small difference between the depth of isopycnal surface ρ^0 and ρ^s along the eastern boundary (in our model this is the same as the difference in mixed layer depth

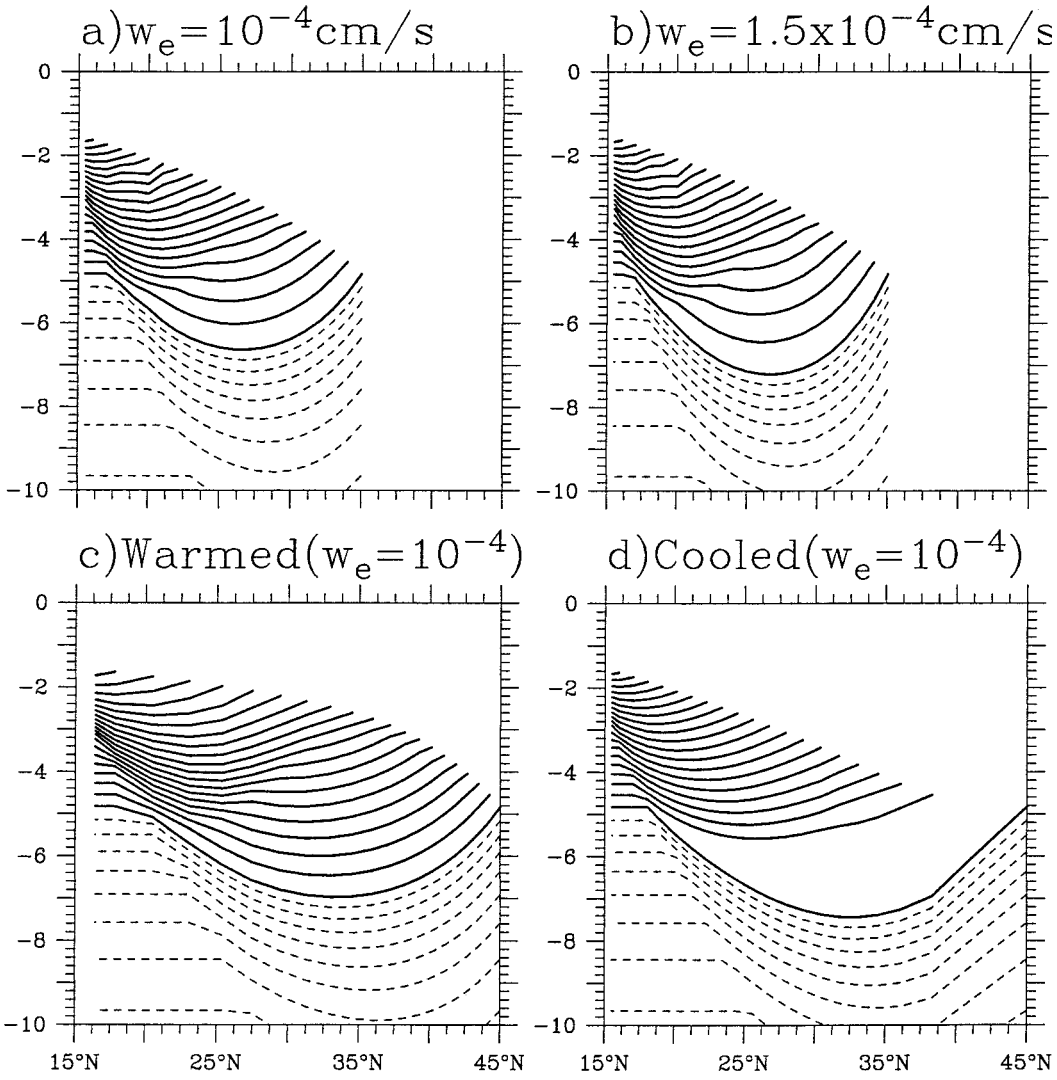

FIG. 11. Isopycnal sections taken along the outer edge of the western boundary (5°E): (a) The intergyre boundary moved to 35°N, with the maximum pumping rate unchanged; (b) the intergyre boundary moved to 35°N, with the maximum pumping rate increased 50% in order to have the same total amount of Ekman pumping; (c) surface warming; and (d) surface cooling.

for the corresponding isopycnals). The final expression for the upper-layer thickness is

$$\Delta z = \frac{2\overline{\rho}\beta\delta y^2}{g\Delta_m\rho^2}\rho_z^a w_e \Delta x. \tag{32}$$

The potential vorticity of the first ventilated layer is

$$q = f\frac{\Delta\rho}{\Delta z} = \frac{g\Delta_m\rho^2\rho_y^s}{2\overline{\rho}\beta\rho_z^a w_d \Delta x\delta y^2}. \tag{33}$$

Note that potential thickness has a quadratic zero along the intergyre boundary. Given the coarse meridional resolution, this is consistent with our numerical solutions shown in Figs. 4c and 4d. Most importantly, from this new relation strong background stratification should lead to low potential vorticity, and this is consistent with solutions shown in Fig. 4.

By examining (30), the thickness of the upper ventilated layer is controlled by two factors as follows. Strong stratification (high potential vorticity) in the unventilated thermocline tends to compress this layer, thus leading to a thin layer, or high potential vorticity in the ventilated thermocline, as discussed by Huang (1988). On the other hand, the thickness of the upper ventilated layer is inversely proportional to the square of the mixed layer depth. Large mixed layer depth leads to a thin ventilated layer because a substantial part of Ekman pumping is used to drive the southward flow in the mixed layer and leaves only a small ''effective pumping'' on the base of the mixed layer. As the mixed layer depth is reduced, the effective pumping on the ventilated thermocline below the mixed layer is substantially increased. As a result, the thickness of the upper ventilated layer increases, as shown in Fig. 4.

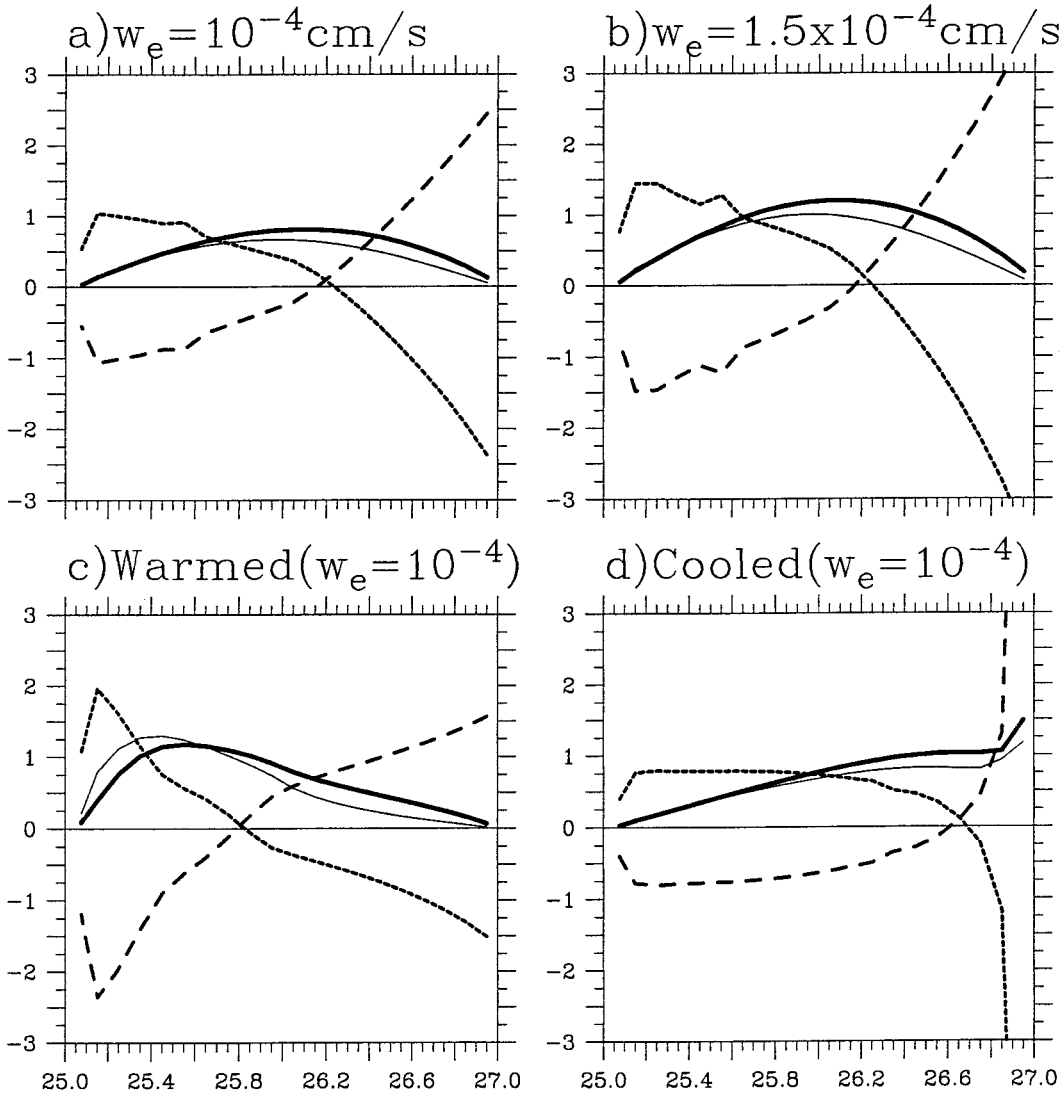

FIG. 12. Subduction rate balance at each isopycnal outcrop band ($\Delta\sigma = 0.1$, in Sverdrups, 10^6 m^3 s^{-1}). The solid lines are the subduction rate, long-dashed lines are the contribution due to the western boundary outflow, the dotted lines are the contribution due to the meridional mass flux convergence, and the thin solid lines are the contribution due to Ekman pumping, $\kappa = 0.3$ cm^2 s^{-1}: (a) the intergyre boundary moved to 35°N, with the maximum pumping rate unchanged; (b) the intergyre boundary moved to 35°N, with the maximum pumping rate increased 50% in order to have the same total amount of Ekman pumping; (c) surface warming; and (d) surface cooling.

d. Special Ekman pumping profile

As discussed above, formation of a low potential vorticity water mass is closely related to the meridional gradient of the Ekman pumping rate. If the meridional gradient of the Ekman pumping rate does not have a maximum near the intergyre boundary, there may not be low potential vorticity water formed near the intergyre boundary. In order to demonstrate this idea we have carried out an experiment in which the Ekman pumping rate is

$$w_e = -1.0 \times 10^{-4}\left(1 - \left|\frac{2(y - y_s)}{y_n - y_s} - 1\right|^{0.5}\right). \quad (11')$$

Note that the meridional gradient of the Ekman pumping rate reaches the basinwide maximum at the middle latitude of the basin instead of at the intergyre boundary (Fig. 6).

Under such a pumping velocity, the model produces a solution where the potential vorticity minimum formed near the intergyre boundary greatly diminishes. This can be seen clearly by comparing the meridional section taken from the model under different Ekman pumping profiles, as shown in Figs. 4c and 7.

To compare results from these experiments quantitatively, we introduce the maximum potential thickness along the western boundary for each isopycnal layer, defined as

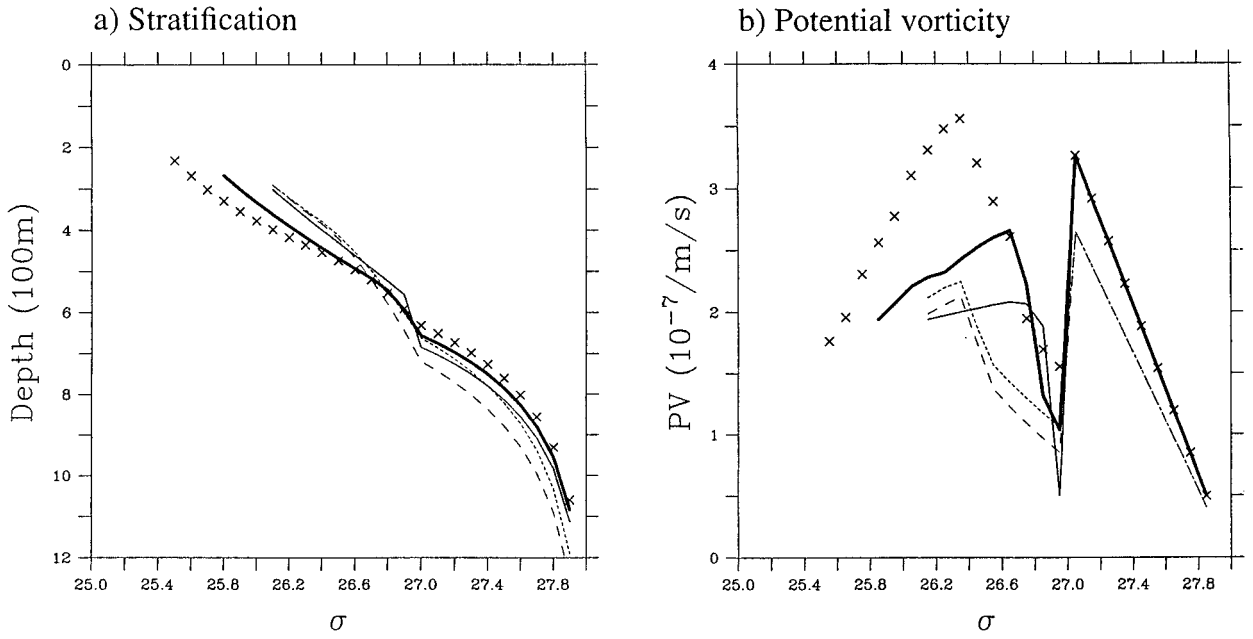

FIG. 13. Density structure taken at a station (26°N, 5°E). The solid line is for the standard case, $w_{e0} = 10^{-4}$ cm s^{-1}; the crosses are for the case with surface warming. The thin solid line is for the case with surface cooling. The thin dotted line is for the case with the intergyre boundary moved to 35°N and $w_{e0} = 10^{-4}$ cm s^{-1}; the long dashed line depicts the cases with the intergyre boundary moved to 35°N and $w_{e0} = 1.5 \times 10^{-4}$ cm s^{-1}.

$$d_p \equiv d\frac{f_0}{f}, \quad \text{taking the maximum for } y_s \le y \le y_{\text{outcrop}}, \tag{34}$$

where d and f are the layer thickness and the Coriolis parameter at a grid point. Here d_p is large for the first outcrop isopycnal, and smaller for other isopycnals. The contrast of d_p between the first outcrop isopycnal and other outcrop isopycnals is sharply increased as κ is gradually reduced. However, for the case with the special Ekman pumping profile labled by 0.1w, the maximum potential thickness is almost constant among the first few outcrop isopycnal layers (Fig. 8).

Note that a low potential vorticity is not necessarily associated with a large volumetric rate of water mass formation. According to the definition, the subduction rate is

$$S_u = -(w_{\text{mb}} + \mathbf{v}_{\text{mb}} \cdot \nabla h), \tag{35}$$

where w_{mb} and $\mathbf{v}_{\text{mb}}$ are the vertical and horizontal velocity at the base of the mixed layer, and h is the mixed depth. Thus, a strong subduction rate is related to the local strength of the Ekman pumping, the horizontal velocity at the base of the mixed layer, and the slope of the mixed layer base.

By integrating the continuity equation over a strip of the mixed layer bounded by two outcrop isopycnals, ρ_1 and ρ_2, in the meridional direction, we have the total subduction rate for each isopycnal interval

$$\int_{x_w}^{x_e} dx \int_{y(\rho_1)}^{y(\rho_2)} S_u \, dy = (U_w - U_e) + (V_n - V_s) - w_e A, \tag{36}$$

where U_w (U_e) are the zonal mass fluxes due to western (eastern) boundary outflow in the mixed layer, V_n (V_s) is the meridional mass flux in the mixed layer, and A is the horizontal area of the strip. As shown in Fig. 9, the total subduction rate is primarily controlled by the Ekman pumping rate. Although the horizontal mass flux terms can be very large, especially near the intergyre boundary, their contributions tend to compensate each other and leave a rather small net contribution to the total subduction rate.

The subduction rate depends on many dynamic factors, such as the local mixed layer depth and its horizontal gradient. In this study, our numerical experiments have been limited to the special cases where the mixed layer depth is set to the corresponding reference level at the eastern boundary. A departure from this assumption may lead to a quite different subduction rate distribution; however, this is out of the scope of this study.

e. Sensitivity to the upper boundary forcing

1) SOUTHWARD MOVEMENT OF THE INTERGYRE BOUNDARY

The position of the intergyre boundary is primarily controlled by the position of the jet stream. Due to

changes in the atmospheric circulation, the position of the jet stream can vary, so the intergyre boundary should change in response. The change of the intergyre boundary can vary over a broad timescale from decades to a millennium. For example, during the last glaciation, the jet stream moved southward and the surface thermal forcing condition was quite different. According to studies on paleo proxies, the structure of the thermocline was remarkably different from that in the present day ocean (e.g., Slowey and Curry 1995). During the last glaciation, the main thermocline was about 100 m shallower, and temperature in the upper 900 m was 4°C lower that of the present day circulation. Similar changes in the jet stream position has also happened within past decades (e.g., Joyce et al. 2000).

In order to see how the structure of the wind-driven gyre changes in response to changes in the position of the intergyre boundary and the surface thermal condition, we carried out four experiments. Since the model's sensitivity to the background stratification has been discussed above, we will assume that the background stratification remains unchanged. In the first two experiments we will move the intergyre boundary to 35°N and assume that the mixed layer density changed linearly from 27.0 at 35°N to 25.0 at 15°N. In the first experiment, we assume that the strength and pattern of the Ekman pumping velocity remain unchanged. However, if we assume that the wind stress associated with the westerlies remains unchanged, the Ekman pumping rate should increase. Thus, in the second experiment the amplitude of the Ekman pumping rate is increased to 1.5 $\times$ 10^{-4} cm s^{-1}.

2) COOLING/WARMING OF THE MIXED LAYER

In the third and fourth experiments, we assume that the intergyre boundary remains at 45°N and the Ekman pumping rate remains unchanged, but the mixed layer density changes. When the surface is warmed, the isopycnal outcrop lines move toward the intergyre boundary, as shown by the long dashed line in Fig. 10. When the surface is cooled, isopycnal outcrop lines move away from the intergyre boundary, as shown by the dotted line.

The structure of the thermocline for these four cases is noticeably different (Fig. 11). The most remarkable difference is shown in the mode water with low potential vorticity formed near the intergyre boundary for the case with a cooler surface condition (Fig. 11d). Note that in this case the meridional gradient of the mixed layer density is much smaller than that in other cases. According to the discussion of (33), the potential vorticity of the first ventilated layer is much lower than that in other cases.

The subduction rate is primarily controlled by the Ekman pumping rate (Fig. 12). For example, when the Ekman pumping rate is increased 50%, the subduction rate is increased in proportion. As discussed above, although the contributions due to meridional and zonal velocity components are large, they tend to compensate each other and give rise to a subduction rate slightly larger than that of the Ekman pumping rate (Figs. 12a,b).

When the surface layer is cooled or warmed, the water mass formation rate (subduction rate) over the isopycnal layers varies accordingly. For example, when the surface layer is warmed, outcrop lines move poleward towards the intergyre boundary, so the area between two outcrop isopycnals decreases. As a result, the total amount of water mass formation within these isopycnal outcrop lines decreases. On the other hand, the water mass formation rate increases for light density ranges (Fig. 12c). However, if the surface layer is cooled, the opposite situation happens, that is, the dense water mass formation rate increases, while the light water mass formation rate declines (Fig. 12d). In the present case, the formation of low potential vorticity is associated with a large volumetric formation rate of mode water.

Changes in the thermocline structure can be seen more clearly through stratification at a fixed position in the basin. For example, stratification profiles taken from a station at the outer edge of the western boundary (26°N, 5°E) show that changes in the stratification have an appearance resembling the second baroclinic mode (Fig. 13a). Since our model is limited to the wind-driven part of the circulation, our discussion about the change in the stratification profile is limited to the base of the wind-driven gyre, roughly the upper one to two kilometers; thus, a warm–cold pattern in the thermocline is equivalent to a warm–cold–null pattern for the whole depth of the ocean, and such a pattern resembles the second baroclinic mode.

Change in the stratification represents a profound change in the potential vorticity distribution. Cooling produces low potential vorticity mode water, while warming produces high potential vorticity mode water, as shown in Fig. 13b. On the other hand, a southward migration of the intergyre boundary implies a larger meridional gradient of the Ekman pumping. As a result, potential vorticity of the mode water declines. The dynamic effects of both cooling/warming and increasing of the meridional gradient of Ekman pumping can be explained using (33). These changes in potential vorticity of the subtropical mode water inferred from our model are consistent with other diagnosis studies based on climatelogical data (e.g., Joyce et al. 2000).

The existence of the second baroclinic mode can be explained as follows. Where the surface is cooled, the temperature in the upper ocean is reduced. As a result, the stratification is weakened. Using a simple reduced-gravity model, it is readily seen that a weaker stratification leads to a deeper interfacial displacement. A downward migration of the interface gives rise to warming at a fixed level. Thus, cooling the surface layer can

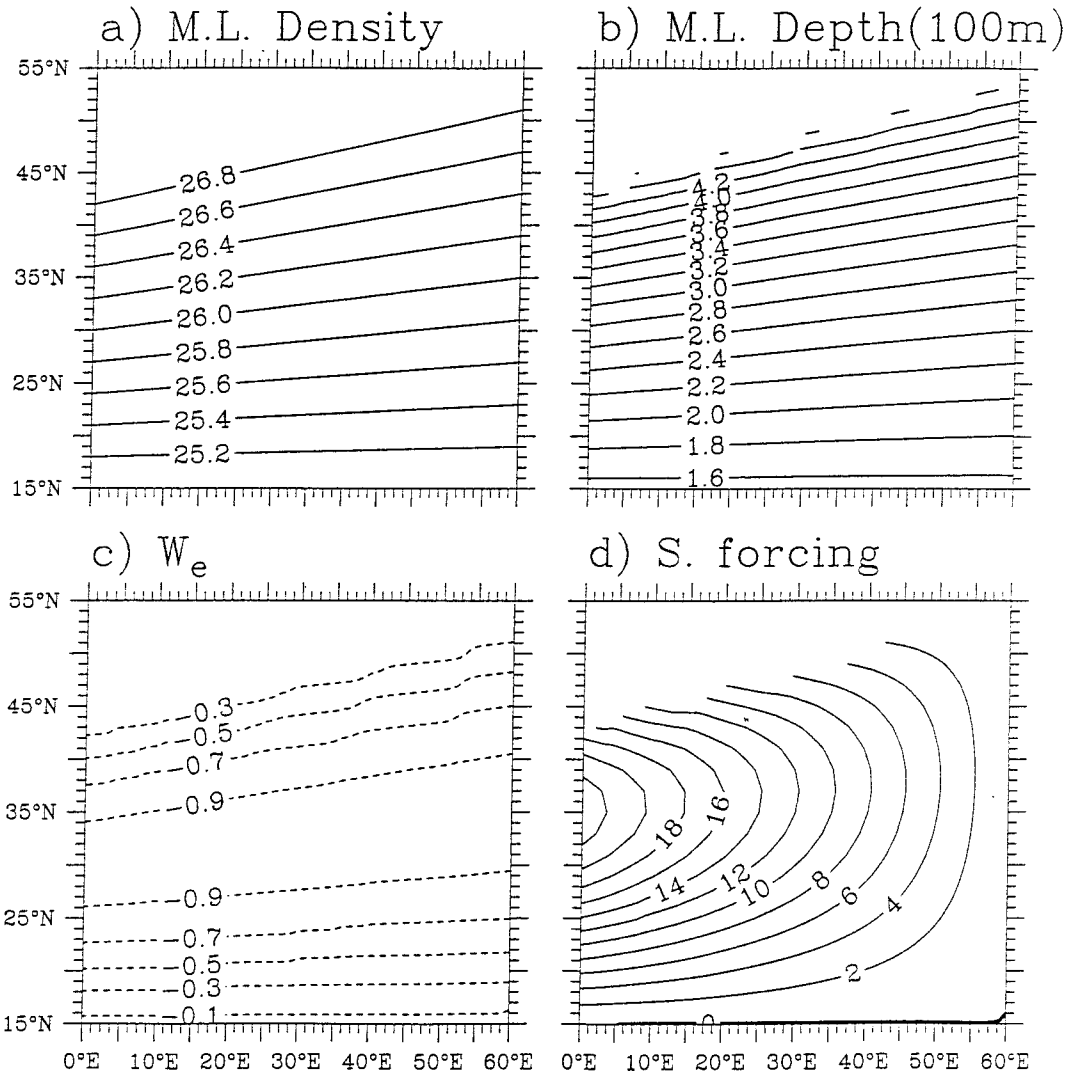

FIG. 14. The upper boundary forcing conditions for a case with a tilted intergyre boundary: (a) The mixed layer density distribution; (b) the mixed layer depth distribution; (c) Ekman pumping rate, in 10^{-4} cm s^{-1}; and (d) the barotropic streamfunction, in 10^6 m^3 s^{-1}.

generalize a perturbation in the form of the second baroclinic mode.

f. Tilting of the intergyre boundary

In the experiments discussed above, the intergyre boundary has been assumed zonally oriented. In the oceans, the intergyre boundary is not zonal. In this section we discuss the effect due to the nonzonal orientation of the intergyre boundary. As an example, we will assume that the intergyre boundary has a NE–SW orientation, and the mixed layer density and depth and the Ekman pumping velocity patterns have similar features (Figs. 14a–c). The corresponding barotropic streamfunction is shown in Fig. 14d. One important feature of the barotropic streamfunction map is that it is nonzero along the intergyre boundary. This leads to a very important dynamic consequence that mode water of very low potential vorticity is formed near the intersection between the intergyre boundary and the western boundary.

Equation (32) can be rewritten as

$$\Delta z = -\frac{2\overline{\rho}\beta\delta y^2}{\Delta_m \rho^2}\rho_z^a M_{bt}, \tag{37}$$

where M_{bt} is the zonally integrated contribution of Ekman pumping

$$M_{bt} = -\int_{x_w}^{x_e} w_e\, dx = -\overline{w_e}(x_e - x_w), \tag{38}$$

where $\overline{w_e}$ is the mean Ekman pumping rate along the latitudinal circle. Since the intergyre boundary is tilted, $\overline{w_e}$ has a finite nonzero value. Thus, for the case with

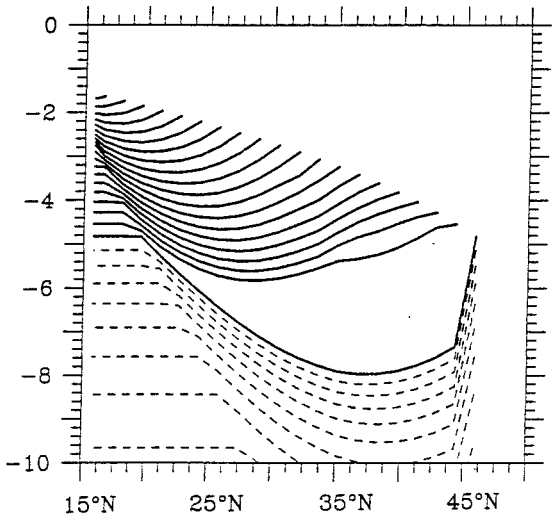

FIG. 15. Meridional section of isopycnal surface taken along 5°E for the case with a tilted intergyre boundary.

a tilted intergyre boundary, the first ventilated layer thickness at the western boundary is finite even if the density interval becomes infinitely small. Accordingly, the potential vorticity for a continuously stratified model is zero near the intergyre boundary, and the corresponding potential thickness at this first ventilated isopycnal is infinite. Since our model treats the continuously stratified ocean in a finite difference form, this singularity in the potential thickness appears in the form of a very thick layer (Fig. 15).

The mode water with very low potential vorticity formed in this case mimics the situation in the oceans, such as the North Atlantic and North Pacific where the intergyre boundary tilting is remarkable (e.g., Huang 1990; Huang and Russell 1994).

4. Conclusions

We have examined the parameter sensitivity of the continuously stratified model for the wind-driven circulation in the upper ocean. Although the model is set up with idealized geometry and forcing, it can provide the essential structure of the wind-driven circulation. Most interestingly, the model's variability under slightly different parameters is relevant to the climate variability observed in the oceans. There are several important issues.

First, given the background stratification the ideal-fluid thermocline model is capable of describing the wind-driven circulation in the oceans. In particular, our model can produce solutions either with finite mixing or with infinitely weak mixing.

Second, the formation of low potential vorticity mode water is directly related to several factors, including the background stratification (or the potential vorticity function for the unventilated thermocline), the meridional density gradient, the meridional gradient of the Ekman pumping rate, and the orientation of the intergyre boundary. On the other hand, the annual-mean subduction rate is controlled by the Ekman pumping rate and the geometry of the mixed layer.

Third, the structure of the wind-driven gyre changes in response to changes in the forcing conditions and the geometric setting of the subtropical gyre, such as a southward migration of the intergyre boundary and the cooling or warming of the surface layer. In general, changes in density structure at a given station appear in a form like the second baroclinic mode.

Finally, the parameter space of the wind-driven circulation is so large that any study can explore a limited part of this space, and many dynamic regions remain to be explored in further studies.

Acknowledgments. This study was supported by the National Science Foundation through Grant OCE-9616950 to the Woods Hole Oceanographic Institution. Reviewers' critical comments have been a great help in clarifying the ideas and presentation.

REFERENCES

De Szoeke, R. A., 1987: On the wind-driven circulation of the south Pacific Ocean. *J. Phys. Oceanogr.,* **17,** 613–630.

Dewar, W. K., 1986: On the potential vorticity structure of weakly ventilated isopycnals: a theory of subtropical mode water maintenance. *J. Phys. Oceanogr.,* **16,** 1204–1216.

Filippov, U. G., 1968: Application of group analysis for the solution of certain ocean flow problems. *Meteor. Hydraul.,* **9,** 53–62.

Huang, R. X., 1988: On boundary value problems of the ideal-fluid thermocline. *J. Phys. Oceanogr.,* **18,** 619–641.

——, 1990: On the three-dimensional structure of the wind-driven circulation in the North Atlantic. *Dyn. Atmos. Oceans,* **15,** 117–159.

——, and S. Russell, 1994: Ventilation of the subtropical North Pacific. *J. Phys. Oceanogr.,* **24,** 2589–2605.

——, and B. Qiu, 1998: The structure of the wind-driven circulation in the subtropical South Pacific Ocean. *J. Phys. Oceanogr.,* **28,** 1173–1186.

Joyce, T. M., C. Deser, and M. A. Spall, 2000: Relation between decadal variability of subtropical mode water and the North Atlantic Oscillation. *J. Climate,* in press.

Ledwell, J. R., A. J. Watson, and C. B. Law, 1993: Evidence for slow mixing across the pycnocline from an open-ocean tracer-release experiment. *Nature,* **364,** 701–703.

Lionello, P., and J. Pedlosky, 2000: The role of a finite density jump at the bottom of the quasi-continuous ventilated thermocline. *J. Phys. Oceanogr.,* **30,** 338–351.

Liu, Z., J. Pedlosky, D. Marshall, and T. Warncke, 1993: On the feedback of the Rhines-Young pool on the ventilated thermocline. *J. Phys. Oceanogr.,* **23,** 1592–1596.

Luyten, J. R., J. Pedlosky, and H. Stommel, 1983a: The ventilated thermocline. *J. Phys. Oceanogr.,* **13,** 292–309.

——, ——, and ——, 1983b: Climate inferences from the ventilated thermocline. *Climatic Change,* **5,** 183–191.

McCartney, M. S., 1982: The subtropical recirculation of mode waters. *J. Mar. Res.,* **40** (Suppl), 427–464.

Oliver, P. J., 1986: *Applications of Lie Group to Differential Equations.* Springer-Verlag, 497 pp.

Rhines, P., and W. R. Young, 1982: A theory of the wind-driven circulation. I. Mid-ocean gyres. *J. Mar. Res.,* **40** (Suppl.), 559–596.

Robinson, A., and H. Stommel, 1959: The oceanic thermocline and the associated thermohaline circulation. *Tellus,* **11,** 295–308.

Salmon, R., 1990: The thermocline as an ''internal boundary layer.'' *J. Mar. Res.*, **48,** 437–469.

Samelson, R., and G. K. Vallis, 1995: Large-scale circulation with small diapycnal diffusion: the two-thermocline limit. *J. Mar. Res.*, **55,** 223–275.

Slowey, N. C., and W. B. Curry, 1995: Glacial–interglacial differences in circulation and carbon cycling within the upper western North Atlantic. *Paleoceanography*, **10,** 715–732.

Stommel, H. M., 1979: Determination of water mass properties of water pumped down from the Ekman layer to the geostrophic flow below. *Proc. Natl. Acad. Sci. USA,* **76,** 3051–3055.

Talley, L. D., 1985: Ventilation of the subtropical North Pacific: The shallow salinity minimum. *J. Phys. Oceanogr.,* **15,** 633–649.

Welander, P., 1959: The thermocline problem. *Philos. Trans. Roy. Soc. London,* **270A,** 415–442.